QUANTITATIVE INFRARED THERMOGRAPHY FOR INFANTILE HEMANGIOMA ASSESSMENT

by

Xinrong You

A thesis submitted to The Johns Hopkins University in conformity with the requirements for the degree of Master of Science in Engineering.

Baltimore, Maryland

May 2014

Abstract

Infrared thermography (IRT) is a promising non-invasive diagnostic tool for characterization of various lesions. It can be used for detection of lesions that can cause abnormality in human metabolic heat generation and blood perfusion, which result in temperature elevation in affected regions. In this research, IRT was used to observe thermal signatures of the infantile hemangioma lesions. Human skin temperature distributions were accurately measured for the lesion and surrounding healthy skin regions. The temperature distributions provide thermal signatures of both surface and subcutaneous lesions that were otherwise invisible with the naked eye. The surface lesion image and the temperature distribution image were combined for simultaneous visualization. Areas associated with elevated temperature contours were calculated for evaluation and comparison of hemangioma evolution between patients' imaging sessions. In both of the patient cases analyzed in follow-up visits, all correspondent areas regressed compared to those recorded during the previous visit.

Advisor:

Dr. Cila Herman

Department of Mechanical Engineering

Johns Hopkins University

Baltimore, Maryland

Reader:

Dr. Arjun Chanmugam

Department of Emergency Medicine

Johns Hopkins University

Baltimore, Maryland

Acknowledgements

I am extremely thankful to Dr. Cila Herman for her advisement.and contribution into this work. I would like to thank Dr. Chanmugam for serving as the second reader of this essay. I am thankful to Dr. Bernard Cohen, Dr. Annie Grossberg and the Johns Hopkins Children's Center for the IRB. I want to thank Mr. Tze-Yuan Cheng and Ms. Akanksha for collecting the infrared thermography data and being a constant source of friendship.

I would not have been able to complete my work without the love and support of my father, Guoyue You, and my mother, Kai Zheng.

Table of contents

List of tables

List of figures

1 Introduction

1.1 Infantile hemangioma

Infantile hemangiomas are the most common tumor that occur in infancy and are found in approximately 10% of the population. Although most infantile hemangiomas are self-involuting, the involution process may take up to several years. Skin hemangiomas are the most common vascular lesion in the pediatric population that can be observed [1], which might seriously affect the patients' cosmetic appearance. Furthermore, if a hemangioma is very large, or develops in a large organ system such as lung, or has uncontrollable bleeding, it could be life-threatening. Treatment is therefore needed for these kinds of hemangiomas.

Treatment of hemangiomas strongly depends on the evolutionary stage of the lesion, which can be classified as: (1) early macular stain, (2) actively proliferating, (3) involuting and (4) involuted hemangiomas [2]. For the purpose of clinical assessment, the following variables are usually taken into consideration: hemangioma color, extension, stiffness with palpation, local complications such as bleeding and ulceration [3]. During the early macular and actively proliferating stages, the extension and proliferation of the lesion is usually rapidly changing, which may not be visible to the naked eye. We thus suggest using infrared thermography (IRT) to follow up the evolution of these lesions by visualizing and quantifying the thermal signature at these stages.

1.2 Infrared thermography

Infrared thermography (IRT) is a sensing method that quantifies the energy radiation emitted by a surface, and thus, can be related to its temperature using appropriate calibration. It relies on

the fact that the thermal energy radiation by a body is proportional to the fourth power of the temperature of the body, which is stated by the Stefan-Boltzmann's law:

$$q = \epsilon\sigma AT^4, \tag{2.1}$$

where ϵ is the emissivity of the surface, σ is the Stefan-Boltzmann constant, A is the surface area of the object, and T is the local absolute temperature of the surface.

Human skin can be modeled by the bioheat equation by Pennes [4]:

$$\rho C \frac{\partial T}{\partial t} = k\nabla^2 T + \rho_b C_b \omega_b (T_b - T) + Q, \tag{2.2}$$

where ρ, C, T, k and Q are the density, specific heat, local temperature, thermal conductivity and the metabolic heat generation per unit volume of the skin, respectively. ρ_b, C_b, ω_b and T_b are the density, specific heat, perfusion rate and arterial temperature of the blood. Therefore, under given environmental thermal conditions, the skin temperature of a given body part depends primarily on the amount of heat transferred by tissue conduction, blood perfusion and metabolic heat generation. Hemangiomas were observed to cause additional metabolic heat generation and blood flow because of the increased vascularity. Therefore, by inspecting changes in skin temperature, IRT is capable of detecting lesions and finding their thermal signatures.

IRT has several exciting features that make it favorable to clinical applications. It is a non-invasive and non-contact diagnostic procedure that helps to quantify, supplement and support clinical observations in terms of temperature differences. Also, this diagnostic procedure can be performed quickly, and can be repeated frequently because there is no radiation hazard involved. Furthermore, the diagnostic results of IRT can be presented by color images, which are usually self-explanatory to patients without the use of complicated medical terminology [5]. The data can then be interpreted for quantification analysis sensitively and specifically.

1.3 Application of infrared thermography for hemangioma assessment

Various imaging techniques have been utilized to investigate hemangiomas that present at different places on the human body. Doppler ultrasonography methods have been used to image capillary hemangiomas, which at the same time also allow the measurement of lesion volume and internal blood velocity [6]. Computed tomography is considered most useful for the imaging of bone hemangiomas, since it shows the radiographic appearances of the lesion, which helps define the extension of the hemangioma [7]. Magnetic resonance imaging has been used to image oral and maxillofacial hemangiomas because it characterizes soft tissue lesion architecture well. 3D reconstructions of hemangiomas have been implemented, through computerized tomography angiography [8], to visualize lesion sizes and vascular flow characteristics.

Saxena et al.[5] applied infrared thermography (IRT) to pediatric imaging of cutaneous hemangiomas for a decade. They confirmed that surrounding the superficial lesion, there's generally a large thermally active region. Kalicki et al. [9] used IRT to assess infantile hemangioma treatment by propranolol. They found an average of 0.9°C and 0.47°C of mean decrease in temperature of the lesion area after treatment. Both Saxena et al. and Kalicki et al. only provided an average temperature differential between the lesion and the healthy skin region. They provided the full infrared image of patients' body parts. But without combining the infrared image with the white-light image, the visual information of the lesion, such as color and ulceration, was not readable on a single image. Also, they did not break the temperature data down to calculate areas of specific temperature elevations. Thus, they missed detailed information about the evolution of the hemangioma.

Given that IRT has attracted a growing interest because of its decreasing cost and complexity in clinical applications, the goal is to take full advantage of high resolution infrared imaging technology to project the thermal signature of the skin hemangioma to the white-light

image. With the semi-transparency of the thermal contours, both the thermal and visual information of the hemangioma should be visible on a single image. Also, quantitative analyses on the thermally active areas are necessary to provide detailed assessment on treatment. Both the visualization and the quantitative process are aimed to provide convenience in clinical diagnosis and in further analysis.

2 Method

2.1 Equipment

The imaging system used in this study consists of a Merlin® midwave infrared camera (FLIR Systems Inc., Wilsonville, OR) and a Canon PowerShot G11™ digital camera (Canon U.S.A., Inc., One Canon Park, Melville, NY). The infrared camera is capable of recording images in the 3-5µm wavelength range and is equipped with a 320x256 pixel indium antimonide (InSb) focal plane array (FPA). With a field of view (FOV) of 22x16 degrees, the infrared camera can record 16-bit raw data at 60 Hz at a temperature sensitivity of 0.025°C.

2.2 Camera calibration

The mid-wave infrared camera was calibrated with a blackbody in the temperature range of 5°C - 35°C temperature as described by Cetingul and Herman (2009)[10]. The blackbody temperature was fitted with a fourth order polynomial to relate to the signal detected by the infrared camera. The exact relationship is given in Appendix I.

2.3 Clinical experiments

The patient studies were conducted at Johns Hopkins Medical Institution's Department of Dermatology at the Outpatient Center in Fall 2009 and at the Johns Hopkins Children Center in Fall 2012.

The imaging procedure began with applying an adhesive paper marker in the proximity of the lesion for each patient. A white-light image of the lesion was then acquired using a digital camera. Under steady conditions, about 20 infrared images were acquired for each case using the infrared camera. The infrared images were taken at the rate of two images per second and were saved in the personal computer using Labview-based image acquisition software.

3 Image processing theory and method

As introduced in Section 2.3, images for each patient are acquired by the infrared camera and the white-light camera. While white-light images show the shape and color of the hemangioma, infrared images provide thermal signatures around lesion sites. It is therefore ideal to combine these two pieces of information to a single image. This combination was achieved by finding the transformation between the coordinates of infrared camera views and the corresponding white-light camera views. The process follows the flowchart below, and will be discussed in this section. All the image processing and visualization procedures were implemented using MATLAB 2013 (Math Works Inc., Natick, MA).

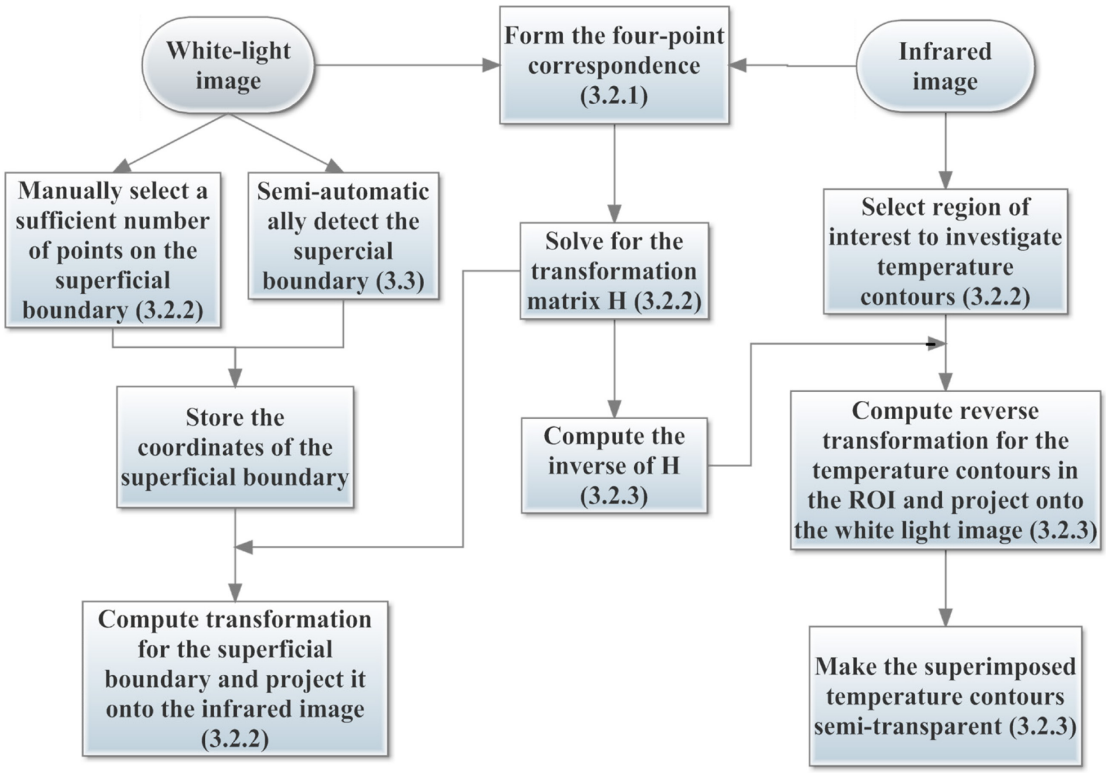

Figure 3.1: Flow chart for the visualization of the superficial boundary of the lesion on the infrared image, and infrared contours superimposed on the white-light image.

3.1 Two-dimensional projective transformation

A two-dimensional projective transformation was applied to find a unique transformation between the two 2D camera coordinates of the same planar object. To apply such a transformation, an assumption must be made that the region of interest (Section 3.2.2) is approximately planar. For a specific point on the object, its coordinates for the two camera views are denoted by vectors $\mathbf{x}$ and $\mathbf{x}'$. Theoretically, the projectivity exists if and only if there is an invertible 3*3 matrix H such that $\mathbf{x}' = \mathrm{H}\mathbf{x}$, which is:

$$\begin{pmatrix} x_1' \\ x_2' \\ x_3' \end{pmatrix} = \begin{bmatrix} h_{11} & h_{12} & h_{13} \\ h_{21} & h_{22} & h_{23} \\ h_{31} & h_{32} & h_{33} \end{bmatrix} \begin{pmatrix} x_1 \\ x_2 \\ x_3 \end{pmatrix}. \tag{3.1}$$

In Equation (3.1), x_1 and x_2 are the x and y components of **x,** and x_1' and x_2' are the x and y components of $\mathbf{x}'$. x_3 and x_3' are usually unity[11]. It should be noted that Equation (3.1) is up to scale, meaning that H can be multiplied by any scaling factor without changing the projective transformation. It results in the fact that such H, which has 9 entries, is with 8 degrees of freedom because of the flexible scaling factor. To solve for H, Equation (3.1) is rewritten into the form $\mathbf{x}' \times \mathrm{H}\mathbf{x} = \mathbf{0}$, which is:

$$\begin{pmatrix} x_2'\mathrm{h}^{3\mathrm{T}}\mathbf{x} - x_3'\mathrm{h}^{2\mathrm{T}}\mathbf{x} \\ x_3'\mathrm{h}^{1\mathrm{T}}\mathbf{x} - x_1'\mathrm{h}^{3\mathrm{T}}\mathbf{x} \\ x_1'\mathrm{h}^{2\mathrm{T}}\mathbf{x} - x_2'\mathrm{h}^{1\mathrm{T}}\mathbf{x} \end{pmatrix} = \mathbf{0}. \tag{3.2}$$

In Equation (3.2), $\mathrm{h}^{\mathrm{i}} = \begin{pmatrix} h_{i1} \\ h_{i2} \\ h_{i3} \end{pmatrix}$, $\mathbf{0} = \begin{pmatrix} 0 \\ 0 \\ 0 \end{pmatrix}$, and the superscript "T" denotes transposition.

Since $\mathrm{h}^{\mathrm{iT}}\mathbf{x} = \mathbf{x}^{\mathbf{T}}\mathrm{h}^{\mathrm{i}}$ for i = 1,2,3, Equation (3.2) can be rewritten as:

$$\begin{bmatrix} \mathbf{0}^{\mathrm{T}} & -x_3'\mathbf{x}^{\mathrm{T}} & x_2'\mathbf{x}^{\mathrm{T}} \\ x_3'\mathbf{x}^{\mathrm{T}} & \mathbf{0}^{\mathrm{T}} & -x_1'\mathbf{x}^{\mathrm{T}} \\ -x_2'\mathbf{x}^{\mathrm{T}} & x_1'\mathbf{x}^{\mathrm{T}} & \mathbf{0}^{\mathrm{T}} \end{bmatrix} \begin{pmatrix} h^1 \\ h^2 \\ h^3 \end{pmatrix} = \mathbf{0}. \tag{3.3}$$

It is observed that among the three equations in Equation (3.3), only two are linearly independent. Therefore, a correspondent pair of points **x** and $\mathbf{x}'$ gives two linearly independent equations. To fully determine H, which has 8 degrees of freedom, four pairs of correspondent points are needed. This algorithm is also known as the four-point algorithm for homography, and is used in this research.

3.2 Image registration and lesion temperature visualization on the white-light image

3.2.1 Image registration

As introduced in Section 3.1, a registration method based on four-point correspondence is used to compute the coordinate transformation between infrared and white-light images. Since a paper marker was kept stationary on the selected body location throughout the data acquisition, it is an invariant object in both views. Any point on the marker can therefore be used for registration. As shown in Figure 3.2, the four corners of the paper marker from both views were selected to form the four-point correspondence. The selection process was accomplished manually.

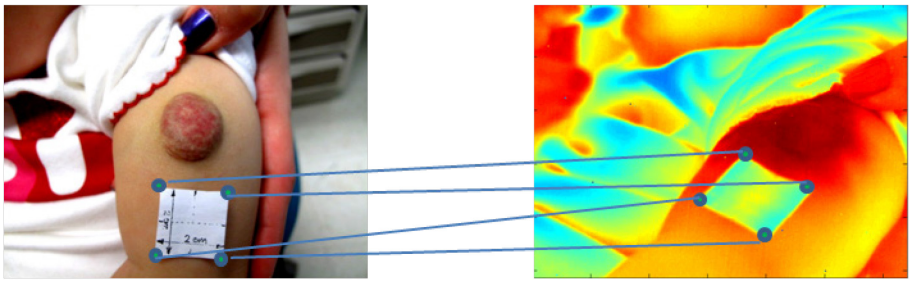

(a) (b)

Figure 3.2: Registration between white-light and infrared images of the hemangioma. The four corners of the marker in both images were identified to form the four-point correspondence. (a) The white-light image of the hemangioma and an adhesive paper marker. (b) The infrared image of the hemangioma and the adhesive paper marker.

It should be noted that it is usually possible to apply an automatic detection algorithm to find points of correspondence of two views of the same object. Such algorithms offer advantages in

terms of the accuracy of registration. This is accomplished by automatically detecting the points, which reduces operator error caused by manual operations, and by running random sample consensus iteration on the results, which further reduces error. However, such algorithms are challenging to implement when the two views have a very large difference in brightness or contrast. Therefore, for two views from a white-light camera and an infrared camera, which have significant changes in colors, it is sufficient to manually complete the registration.

3.2.2 Visualize the superficial boundary of the lesion in the infrared image

The 2D homography transformation from white-light to infrared view is obtained first. Based on the correspondent pixels selected in registration, an equation similar to Equation (3.1) is formed to accomplish this transformation as $P_i = HP_w$, or:

$$\begin{bmatrix} x_i^{(1)} & x_i^{(2)} & x_i^{(3)} & x_i^{(4)} \\ y_i^{(1)} & y_i^{(2)} & y_i^{(3)} & y_i^{(4)} \\ 1 & 1 & 1 & 1 \end{bmatrix} = \begin{bmatrix} h_{11} & h_{12} & h_{13} \\ h_{21} & h_{22} & h_{23} \\ h_{31} & h_{32} & h_{33} \end{bmatrix} \begin{bmatrix} x_w^{(1)} & x_w^{(2)} & x_w^{(3)} & x_w^{(4)} \\ y_w^{(1)} & y_w^{(2)} & y_w^{(3)} & y_w^{(4)} \\ 1 & 1 & 1 & 1 \end{bmatrix}. \quad (3.4)$$

The subscripts “i” and “w” in Equation (3.4) denotes infrared and white-light, respectively; superscripts “(1)” through “(4)” denote the correspondent pixels selected in sequence. For each pixel coordinates, the third dimension coordinate is assumed to be unity [11]. Following the normalized direct linear transformation algorithm discussed in sections 4.1 and 4.4 of Hartley and Zisserman[11], Equation (3.4) can be solved for the transformation matrix H.

After the transformation matrix H is determined, the superficial boundary of the hemangioma, which is only visible in the white-light image (Figure 3.3(a)), is projected onto the IR image (Figure 3.3(b)) for comparison. The boundary is manually outlined by a sufficient number of discrete points on the superficial boundary of Figure 3.3(a). The corresponding

location of those points in the IR image are computed using Equation (3.1). They are displayed as green dots in Figure 3.3(b). A semi-automatic detection algorithm to outline the boundary will be discussed in Section 3.3.

In the next step, a region in the infrared image is selected such that it contains detailed temperature information on the superficial lesion and its surrounding area. The region is represented by a black box shown in Figure 3.2(b), which serves as the region of interest (ROI) in the subsequent quantitative analysis.

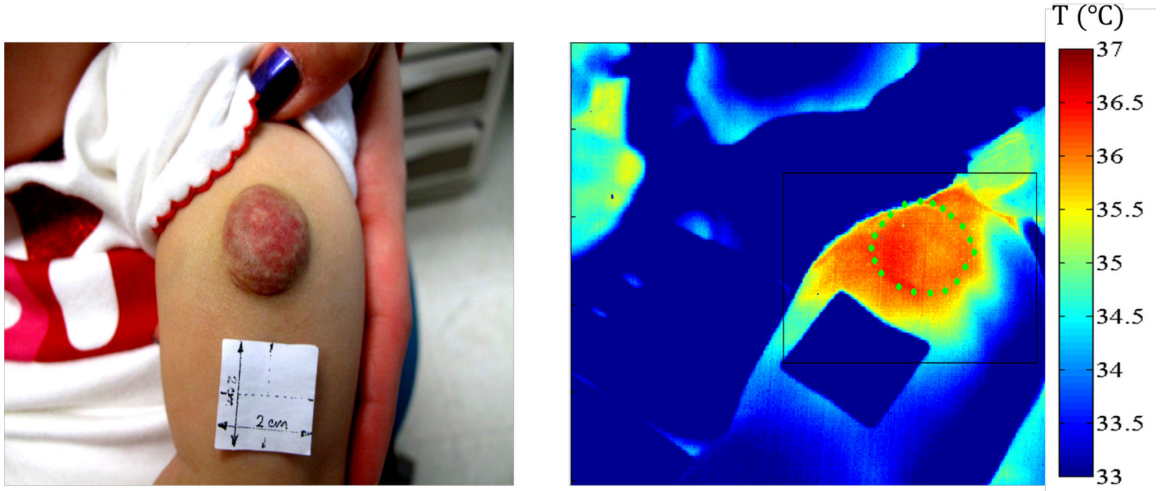

(a) (b)

Figure 3.3: Finding the superficial lesion boundary on the infrared image. (a) White-light photograph of the hemangioma including a white 2cmx2cm paper marker. (b) Infrared thermographic image with The ROI represented with the black box, and the hemangioma's superficial boundary represented with the green dots.

3.2.3 Visualizing the thermal signature of hemangioma on the white-light image

To further visualize the thermal signature of the hemangioma in infrared view, the black box area (ROI) in Figure 3.3(b) is investigated. Thermal contours with a temperature range from healthy skin temperature to the highest temperature present in the image are shown in Figure 3.4(a).

Human skin temperature depends primarily on the amount of heat transferred by tissue conduction, blood perfusion, metabolic heat generation, and environmental thermal conditions. These conditions varied between imaging sessions due to the change in thermal characteristics of the hemangioma as well as differences in ambient conditions on the day of imaging. Therefore, the healthy skin temperature must be determined for each case and each visit. One way to find the healthy skin temperature is to locate the symmetric counterpart of the location where the lesion presents. In cases where symmetric counterparts are not available within the data, healthy skin temperature is carefully determined by averaging temperature over a certain area visible in the thermal image. Such area should be far away from the lesion so that its temperature doesn't appear elevated due to the lesion. The area should not be too far away so that it remains on approximately the same body part as the lesion.

In order to project the temperature contours in Figure 3.3(a) onto their corresponding locations in the white-light image, a reverse transformation is required. As mentioned in Section 3.1, the transformation matrix H in Equation (3.1) is invertible. Therefore, given any pixel in the infrared image, P_i, its corresponding pixel in the white-light image, P_w, can be computed by:

$$P_w = H^{-1}P_i\,. \qquad (3.5)$$

Once the temperature contours of the ROI are computed, their corresponding pixels in the white-light image are obtained via Equation (3.5). Using the pixel coordinates obtained in this way, the white-light image is then overlaid with color contours representing ranges of skin temperature. The contours are made semi-transparent, which finally results in Figure 3.3(b). Details of the mapping procedure can be found in Appendix I.

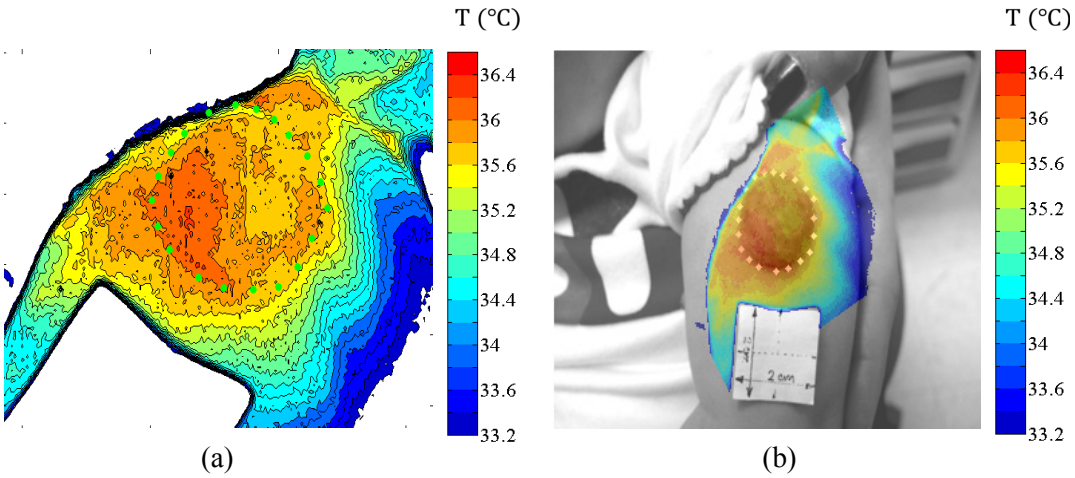

Figure 3.4: The temperature contours overlaid onto the white-light image. (a) The temperature contour of the ROI using 33.2°C as the healthy skin temperature. Each contour represents a 0.2°C deviation from the neighboring contour. (b) White-light photograph with superimposed semi-transparent temperature contours and the superficial boundary of the hemangioma demarcated with twenty white dots.

3.3 Semi-automatic segmentation of the superficial boundary

An image segmentation method was developed to outline the superficial boundary of the lesion, in place of the previously described method of representing the boundary with dots.

To optimize the calculation, a template is manually chosen on the white-light image (represented with a black box in Figure 3.5(a)) such that it is just big enough to contain the full superficial lesion. Since the lesion in the template differs greatly in contrast from the background, changes in grayscale contrast can be detected by operators that calculate the grayscale gradient. Taking advantage of this, the lesion boundary can be segmented following a routine segmentation method [12] (Figure 3.5(b)). Next the segmented boundary is transformed from inside the template to the corresponding position in the original image. Finally, it was overlaid onto the white-light image using the red color (Figure 4(c)). A detailed description of segmentation can be found in Appendix I.

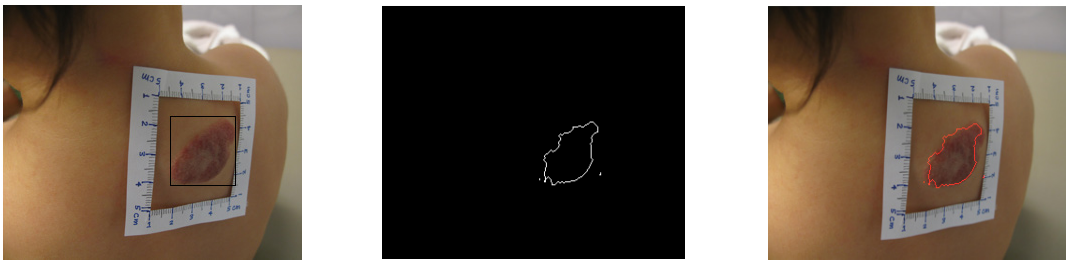

(a) (b) (c)

Figure 3.5: Segmentation of the superficial boundary of the lesion. (a) Black box representing the template chosen for segmentation. (b) Segmented superficial boundary of the lesion and (c) the red boundary representing the segmented lesion boundary overlaid onto the original image.

3.4 Area calculation

To monitor the evolution of the hemangioma over time as an indicator of treatment progress, areas of affected region are measured. It is most convenient to calculate the total area of the region with temperature above a specific temperature value.

The total area warmer than a given temperature value can be calculated, either from the infrared image temperature profile directly, or from temperature profile transformed back onto the white-light image. Both methods can be used to compare the relative areas of regions with different temperature elevations. In order to convert the area in units of pixels to real dimensions, both the marker and the area affected by the lesion on the image should not be distorted. Among the available data, the white-light image usually satisfies this condition, while the infrared image does not. Therefore, it was preferred to calculate the areas from the infrared image superimposed to the white-light image.

If the areas were to be measured in the infrared image, simply counting the number of pixels that represent each contour would be sufficient. However, after transforming the coordinates from the infrared to the white-light image using 2D projective transformation, contours are linearly projected to their corresponding locations in the white-light image, and some blank pixels would appear due to stretching (as is shown in Figure 3.6 below). Therefore, it was not convenient to continue with this method in the white-light image without knowing exactly to which contour each of the blank pixels belonged.

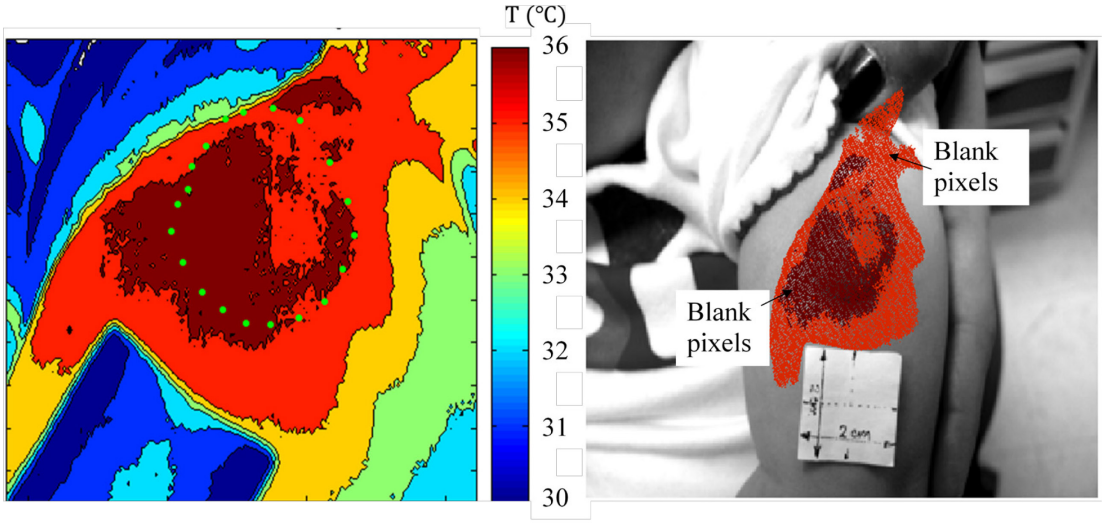

(a) (b)

Figure 3.6: Blank pixels in temperature contours on the white-light image. (a) The temperature contours obtained from the infrared image, no blank pixels. (b) Highest two temperature contours of (a) transformed to their corresponding locations in the white-light image. In the middle of each contour, numerous blank pixels are observed due to projection mismatch and stretching.

One alternative method to counting pixels is to calculate the area of the polygons formed by the transformed contour lines.

3.4.1 Transformation of the temperature contour lines

Temperature contour lines of the hemangioma site were obtained for each case from the infrared images using the MATLAB function “contour”, with temperature ranging from the healthy tissue temperature to the highest temperature present in the lesion. Similar to the transformation of temperature contours from infrared to the white-light image in Section 3.2.3, using Equation (3.4), pixel coordinates of those representing contour lines were transformed to find their corresponding pixels in the white-light image. For example, to investigate the areas that

were with temperature higher than 35.2°C and 36.2°C, respectively, of the temperature profile given in Figure 3.7(a), the contour lines were extracted and were shown in Figure 3.6(b). Subsequently, the contour lines were transformed to their corresponding locations on the white-light image, as shown in Figure 3.6(c).

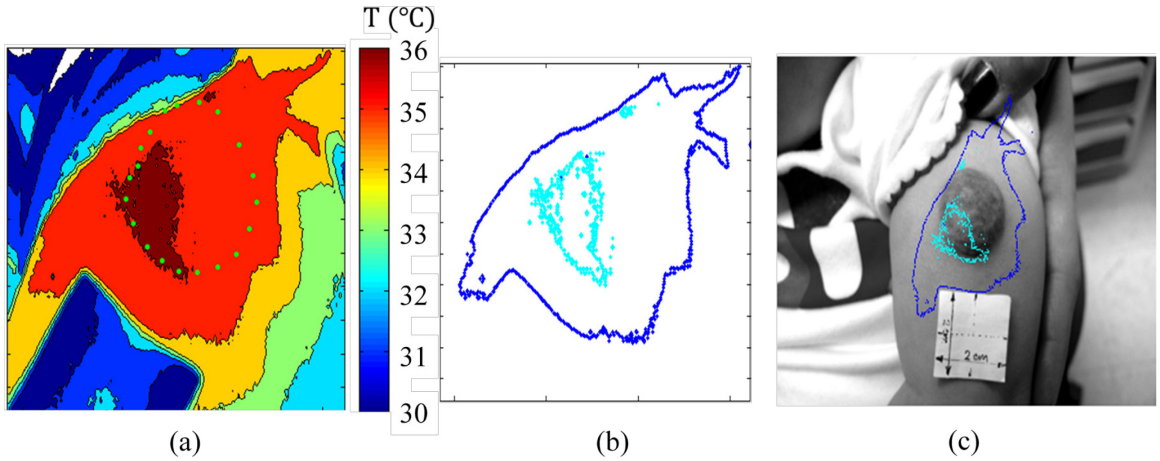

Figure 3.7: Temperature contour lines projected onto the white-light image. (a) Temperature contour in the infrared image. (b) Contour lines of temperature 35.2°C and 36.2°C extracted from (a). (c) Contour lines in (b) transformed and plotted on the white-light image.

3.4.2 Calculation of the contour areas in units of pixels

After projecting the contour lines to the white-light image, the pixels that represent contour lines become discrete due to stretching. The area of a contour can be approximated by area of the polygon formed by connecting neighboring pixels on the contour line. The coordinates of the pixels that represent a contour line can be obtained using the MATLAB function "contour". However, the default order of the pixels delivered by the "contour" function does not always place neighboring pixels together. This is illustrated in Figure 3.8(a) and (c), where the pixels represent a contour line are connected head-to-tail, following the default order of the output

matrix. Computing the area of the polygon formed in such a way would lead to erroneous results. Therefore, the pixels must be sorted properly before the area calculation.

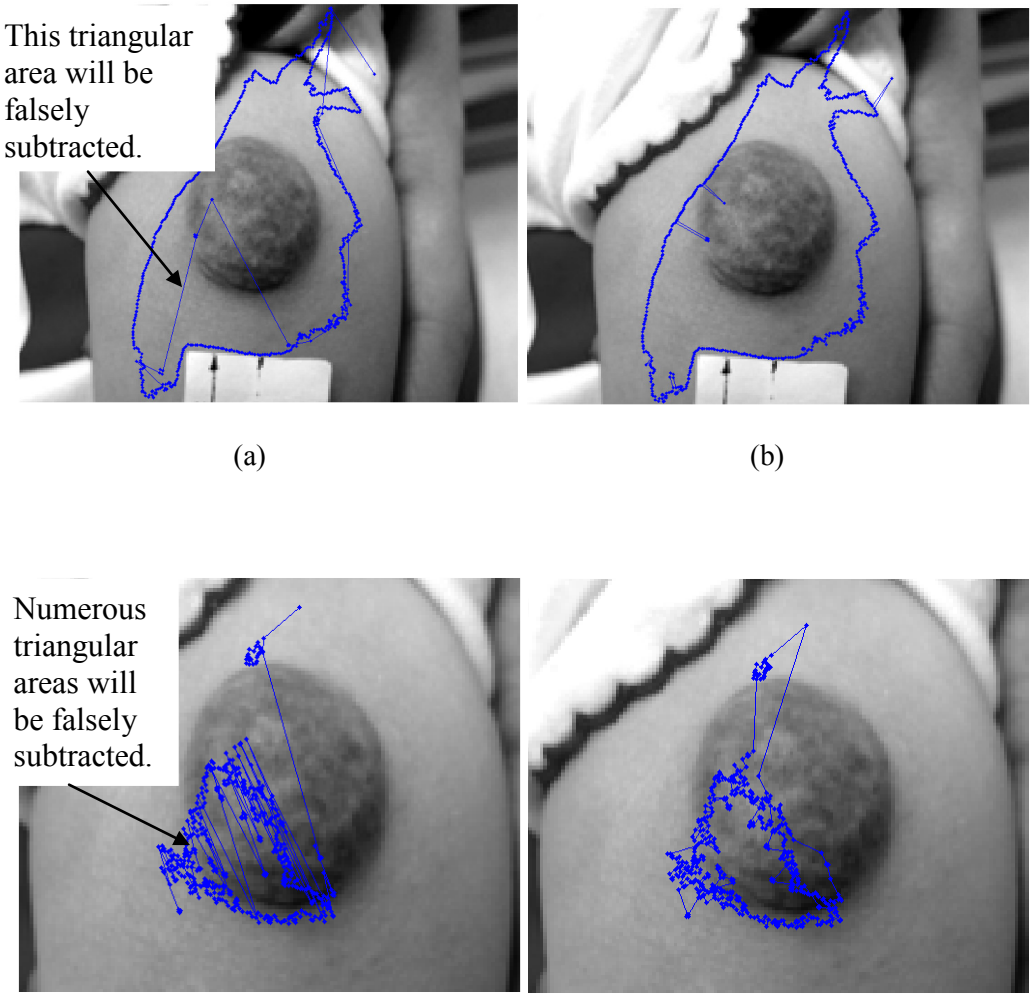

Figure 3.8: Comparison between the areas formed by the pixels in the original order and the correct order after sorting. Data were taken from the case S48. (a) The contour line of 35.2°C, pixels connected in the original order. The triangular area shown by the arrow will be subtracted due to the wrong order. (b) Contour line of 35.2°C, pixels connected in correct order after sorting. (c) Contour line of 36.2°C, pixels connected in the original order. Numerous erroneous

subtractions occurred in the area shown by the arrow. (d) The contour line of 36.2°C, pixels connected in correct order after sorting.

It is a challenging task to recover the correct order of the pixels on the contour line from the output matrix. However, the pixels can be sorted to create a new order that approximates the correct order. Such a sorting problem is similar to the Travelling Salesman Problem (TSP) in optimization. It states: "Given a list of cities and the distances between each pair of cities, what is the shortest possible route that visits each city exactly once and returns to the origin city?"

Several algorithms were developed to solve the problem, varying from brute force method (computation time O(n!)) to the k-opt algorithms (computation time O(n)). Balancing the difficulty of implementation and computational cost, an heuristic algorithms based on the convex hull (computation time $O(n^2 \log_2(n))$ [13] was chosen to be implemented. In this study, the convex hull heuristic algorithm implements the following steps:

1) Find the convex hull of all the transformed pixels that represent the desired contour line, using Graham scan [14] (An introduction to the convex hull and the Graham scan can be found in Appendix II). Define the convex hull as the original subtour.
2) Select a pixel of the contour line that is not in the subtour. Find an edge in the subtour such that the cost of inserting this pixel between the edge pixels will be minimal. Insert the pixel in between the edge pixels to form the new subtour.
3) Repeat step 2) until the subtour covers all pixels.

After the pixels have been sorted, by connecting neighboring pixels, it could be observed that the polygon was formed as desired (Figures 3.8(b) and (d)). The area calculation would carry much less error compared to the analysis without sorting.

3.4.3 Conversion of the area from pixels to the real dimensions

To reduce the conversion errors in the white-light image, the lesion site and the paper marker used for the geometrical calibration should be in the same plane normal to the camera axis. For images that satisfy this condition, the square area in the white-light image (shown in Figure 3.9) is manually selected. The area of the marker in units of pixels is then computed from the square area. In this case, since the marker size is known ($2\ cm \times 2\ cm$), the conversion factor (CF) that converts area from units of pixels to real dimensions can be found as:

$$CF = Area_{Marker,Pixels} / Area_{Marker,Real}. \tag{3.6}$$

The real size of each contour area can then be calculated by dividing the area measured in pixels by the conversion factor CF.

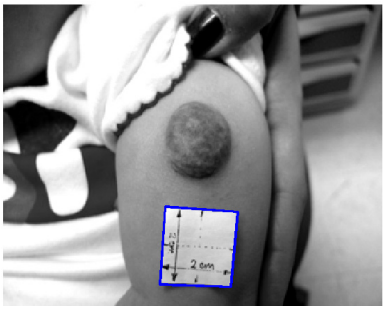

Figure 3.9: Computation of the conversion factor. Marker size in units of pixels is computed by selecting and calculating the area shown with the blue square, which outlines the marker. Then the marker size in pixels was divided by its known real size to get the conversion factor.

4 Results

4.1 Visualization of the thermal signature of hemangiomas on the white-light image

Patient with two documented imaging sessions: S24 and S48

Patient S48 "was a 16-month-old, Caucasian female at the time of imaging. She had a 2cm mixed, focal hemangioma on the left arm and was treated with Propranolol prior to imaging. The hemangioma was described as a 'nodular red vascular plaque with some central graying' on the day of imaging [15]".

As shown in Figure 4.1(b) on the next page, overlaying temperature contours of the ROI onto the white-light image allows both the superficial lesion area and the temperature-elevated lesion area to be viewed simultaneously superimposed to each other. It was observed that the superficial lesion was generally entirely dark red. It was also observed from Figure 4.1(b) that the highest temperature elevation was detected on the left-bottom part of the lesion. The thermally active region was larger than the superficial lesion size. Also, from contour plot of the thermally active region, it was observed that the hemangioma had major thermal extensions to its lower left and the top regions (higher than 36°C). This observation is obvious when the line of each temperature contour is displayed in section 4.2.

The healthy skin temperature is computed by averaging the temperature pixel data for the region indicated by the arrow in Figure 4.1(c). The healthy skin temperature was 33.2(±0.1)°C. The affected region had a maximum temperature of 36.5°C.

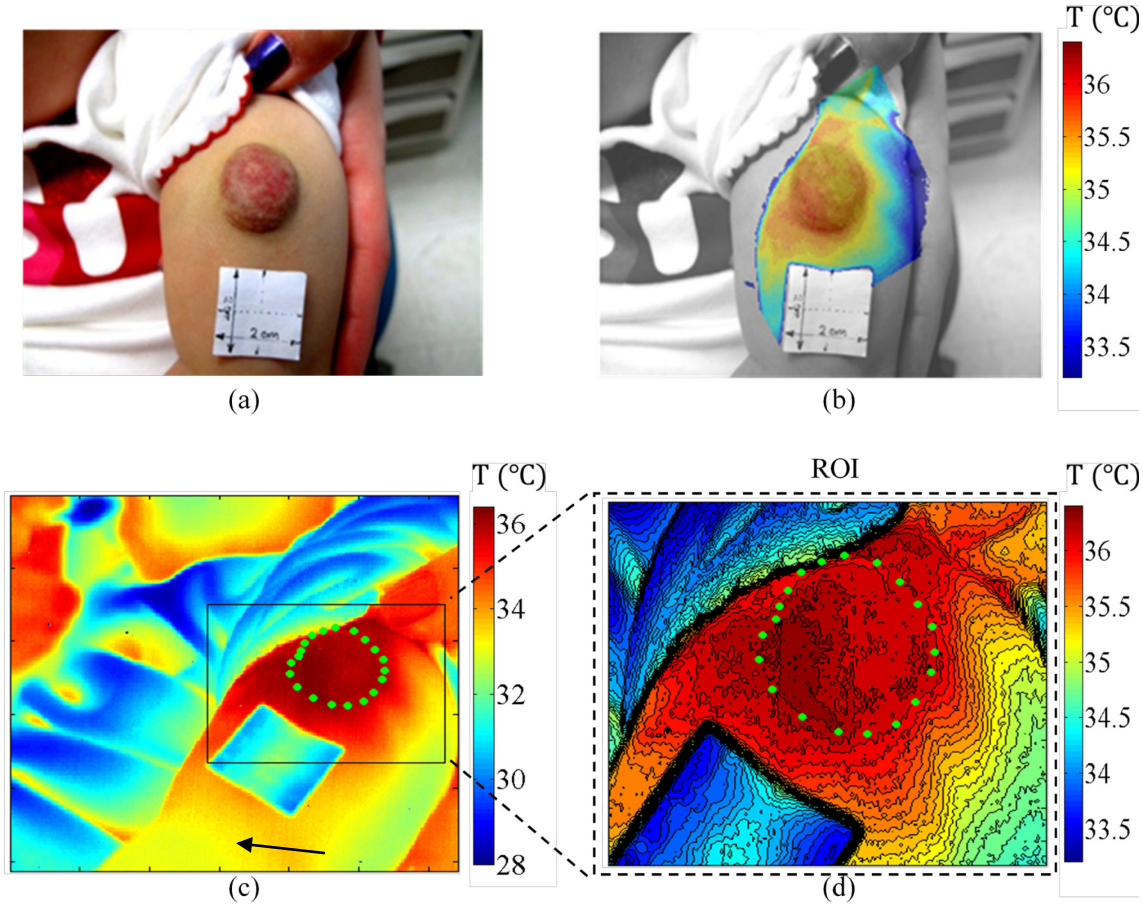

Figure 4.1: Thermal signatures of the lesion of Patient S48. (a) White-light image, (b) white-light image overlaid with temperature contours within the ROI, (c) infrared image with the box indicating the ROI. The arrow shows the approximate region where the temperature was averaged and was taken to represent the healthy skin temperature, (d) Temperature contours in the ROI.

Figure 4.2 on the next page is from the imaging session data of S24, which is the previous imaging session of S48 of the same patient. From Figure 4.2(b), the affected region was larger than the superficial lesion size. The thermally elevated portion of the hemangioma (areas with temperature above 36°C) was clearly visible on the left and top regions of the superficial lesion. This was consistent with the observation of S48 in general. The changes in areas of contours can be further analyzed, and the results will be shown in Section 4.2.

The healthy skin temperature of this case was computed as 32.9(±0.1)°C. The affected region of the lesion had a maximum temperature of 36.4°C.

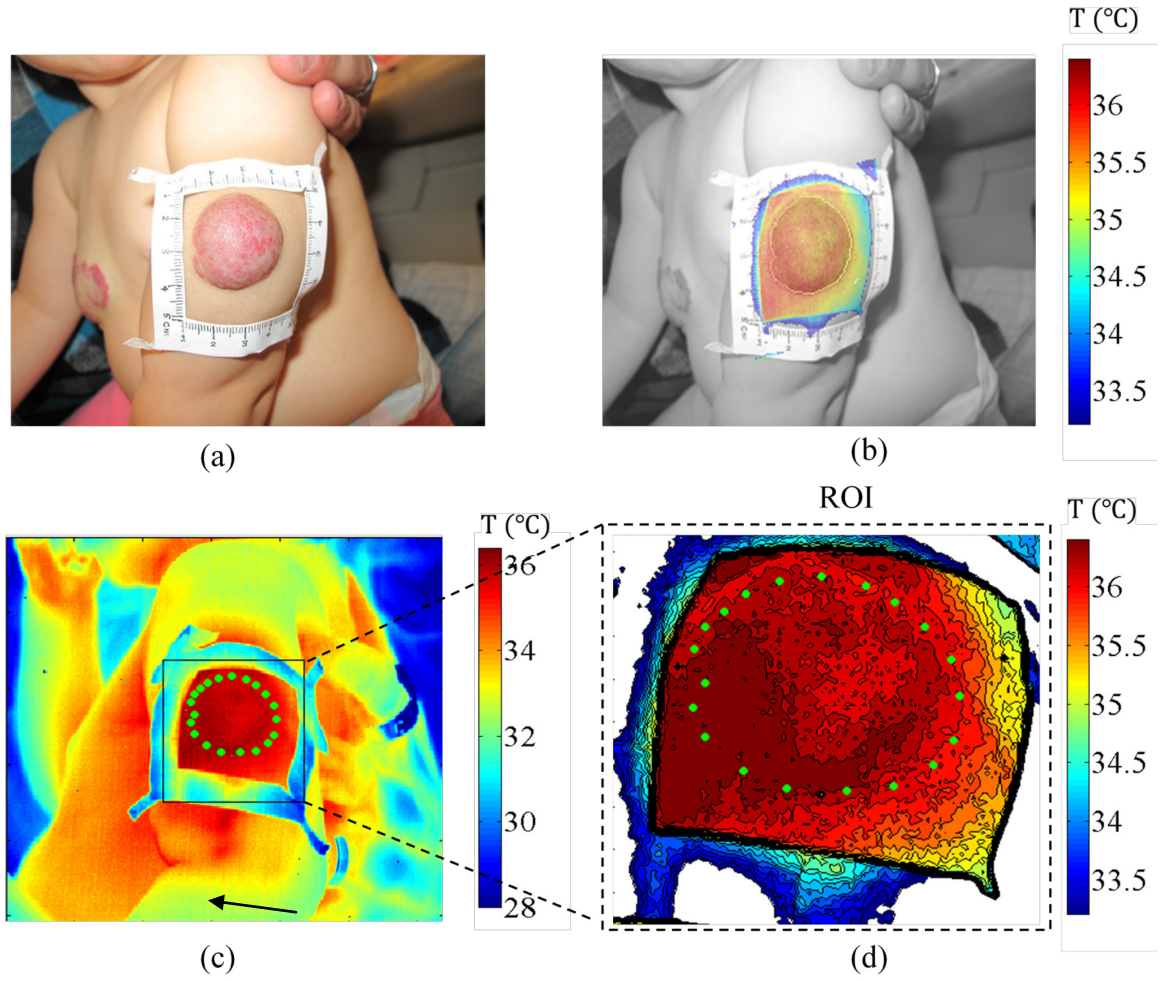

Figure 4.2: Thermal signatures of the lesion of Patient S24. (a) White-light image, (b) white-light image overlaid by temperature contours within the ROI, (c) infrared image with the box indicating the ROI. The arrow shows the approximate region where the temperature was averaged and was taken to represent the healthy skin temperature. (d) Temperature contours in the ROI.

Patient with two documented imaging sessions: S20 and S39

Patient S20 "was a 29-month-old, Caucasian female at the time of imaging. She had a 3cm deep, focal hemangioma on the glabella and had received propranolol treatment prior to imaging. The hemangioma was described as a 'soft compressible subcutaneous nodule with an overlying purple hue and some coarse overlying telangiectasia' [15]".

There was obvious purple hue on the hemangioma as shown in Figure 4.3(a) on the next page. From Figure 4.3(b), it follows that the purple hue approximately coincides with the region where the hemangioma was most thermally active. The superficial lesion size was larger than the thermally active region. Also, there was no noticeable thermally elevated portion of the lesion outside of the superficial lesion.

The healthy skin temperature was computed as 34.2(±0.1)°C. The affected region of the lesion had a maximum temperature of 36.0°C.

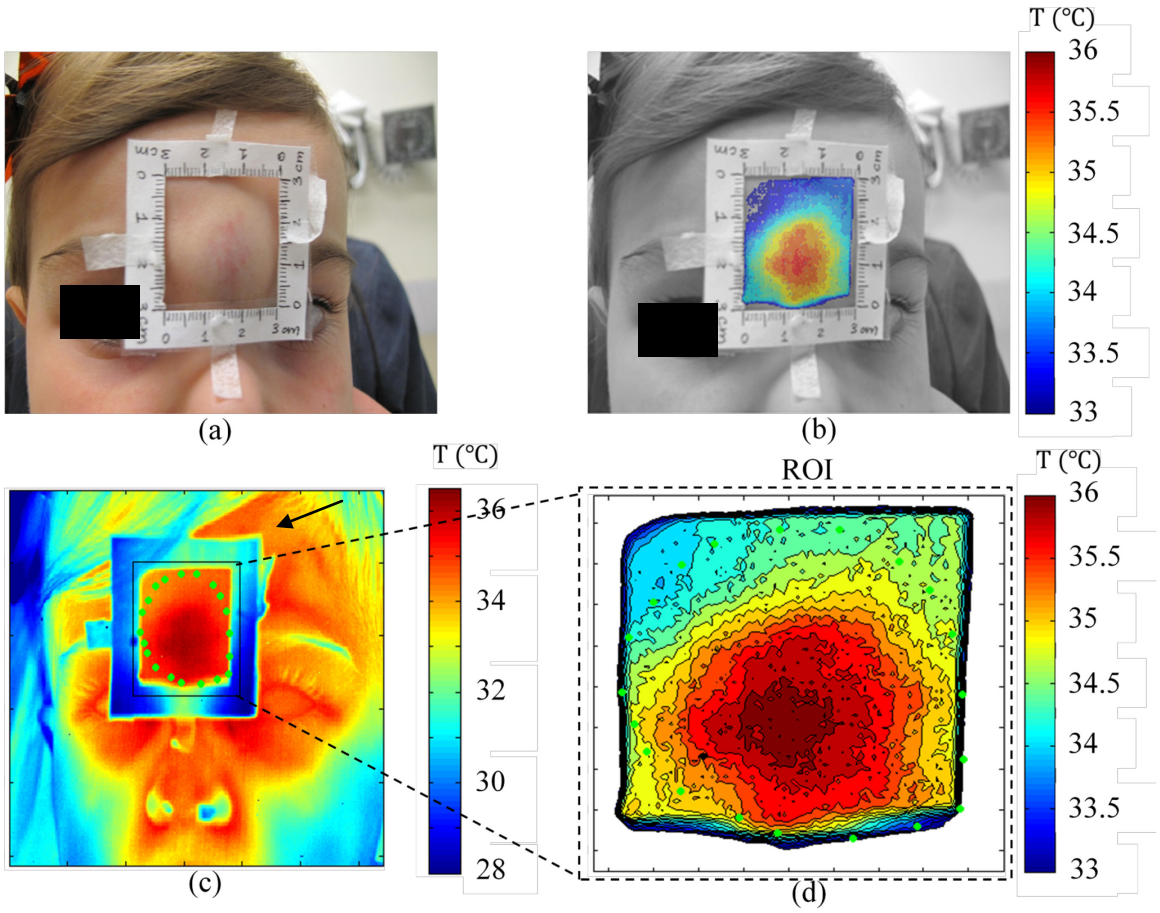

Figure 4.3: Thermal signatures of the lesion of Patient S20. (a) White-light image, (b) white-light image overlaid with temperature contours within the ROI, (c) infrared image with the box indicating the ROI. The arrow shows the approximate region where the temperature was averaged and was taken to represent the healthy skin temperature. (d) Temperature contours in the ROI.

Figure 4.4 below is patient S39, which was the latter imaging session of S20 of the same patient. From Figure 4.4(b), the general shape of thermally active region was consistent with the previous imaging session (Figure 4.3(b)). The lesion size was larger than the thermally active region, and there was no thermal extension of the hemangioma out of the superficial lesion region. The healthy skin temperature was computed as 33.9(±0.1)°C. The thermally active region of the lesion had a maximum temperature of 35.8°C.

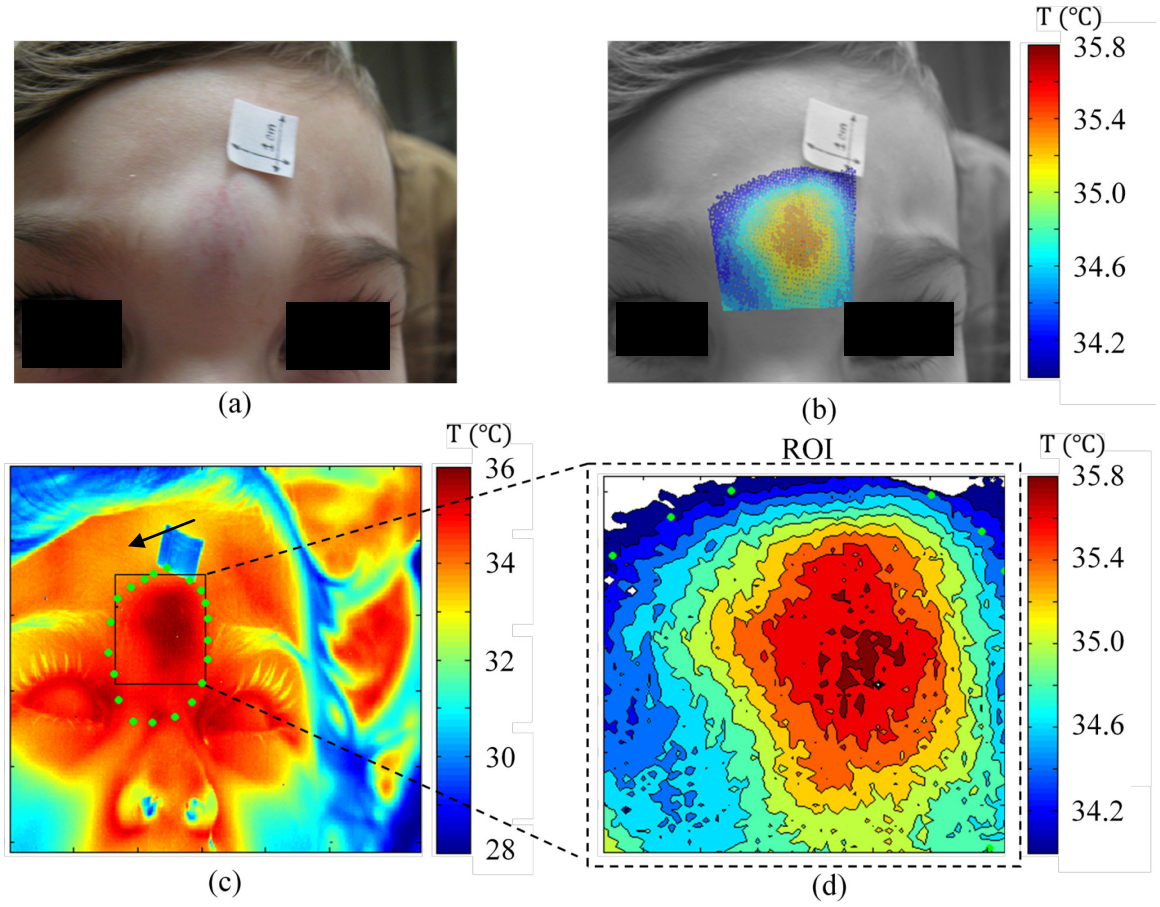

Figure 4.4: Thermal signatures of the lesion of Patient S39. (a) White-light image, (b) white-light image overlaid by temperature contours within the ROI, (c) infrared image with the box indicating the ROI. The arrow shows the approximate region where the temperature was averaged and was taken to represent the healthy skin temperature. (d) Temperature contours in the ROI.

4.2 Contour area calculation and comparison between imaging sessions

Contour areas in the thermally active regions were calculated for the two patients listed in Section 4.1. Areas in unit of pixels were first computed in the white-light image scale. The conversion factor was calculated using Equation 5. Then the areas were converted to real sizes. Table 4.1 below shows the conversion of contour areas for the case S48.

Table 4.1: Conversion of contour areas in pixels to real dimensions (case S48).

Total area with temperature higher than (°C)	**35.80**	**35.95**	**36.10**	**36.25**	**36.40**	**Marker**
Area (pixels)	5529	4068	2701	700	117	3940
Area (cm^2)	5.6	4.1	2.7	0.71	0.12	4

(Conversion factor: 985 pixels/cm^2)

The same procedure was repeated for the conversion of contour areas in pixels to real dimensions for the case S24, which is the previous imaging session of S48. Areas were calculated in correspondence to the contours as shown in the Figure 4.5 on the next two pages.

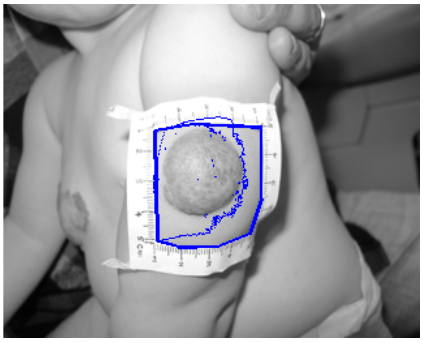

(a)

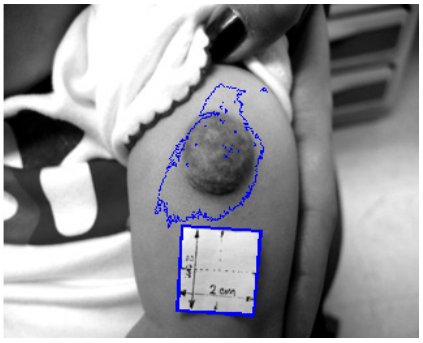

(b)

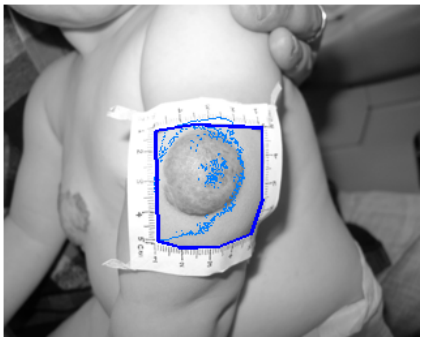

(c)

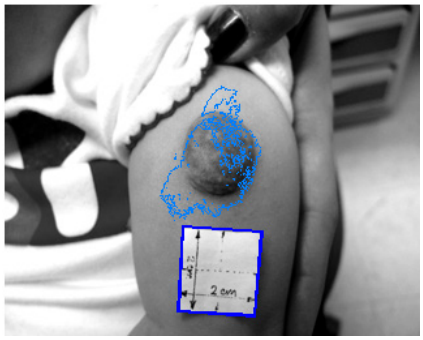

(d)

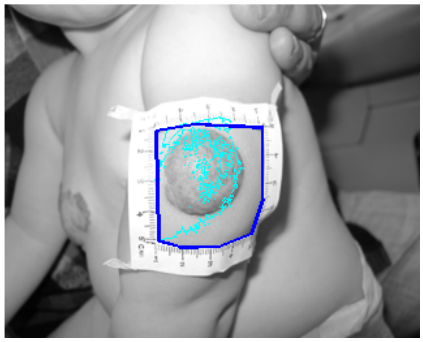

(e)

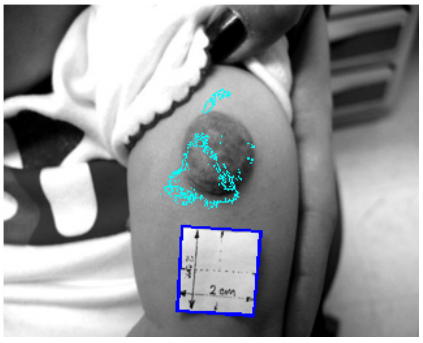

(f)

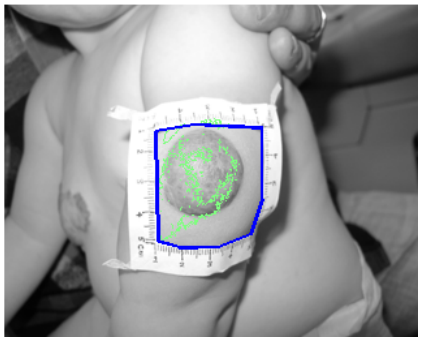

(g)

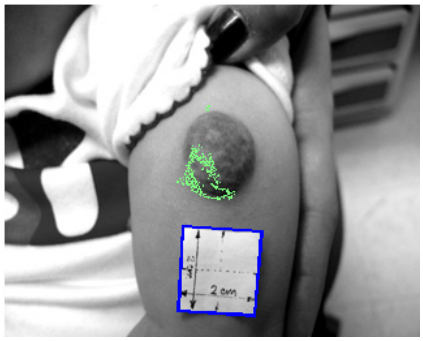

(h)

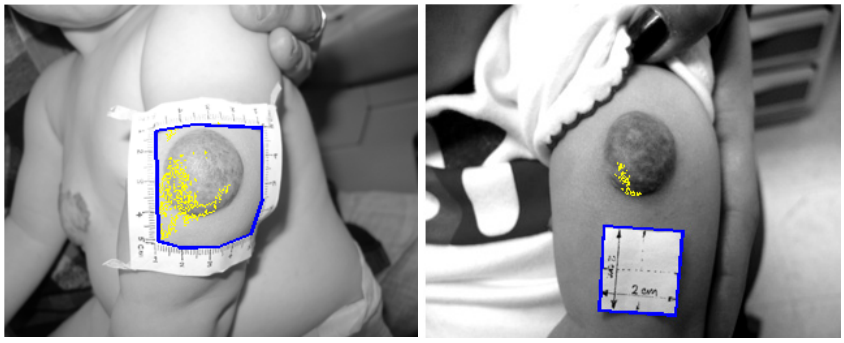

(i) (j)

Figure 4.5: Areas comparison of Patient imaging sessions S24 and S48. Area in pixels was calculated for each of the contours above. Contour lines in Figure(a)(c)(e)(g)(i) represent contour areas of Patient S24 with temperature above 35.50°C, 35.65°C, 35.80°C, 35.95°C, 36.10°C, respectively. The area in pixels of the square box shown in blue was calculated as the marker area in pixels. Figure(b)(d)(f)(h)(j) represent contour areas of Patient S48 with temperature above 35.80°C, 35.95°C, 36.10°C, 36.25°C, 36.40°C, respectively. Each pair of figures in a row is showing contours at the same level of relative temperature elevation (compared to healthy skin temperature) of both cases.

As mentioned in Section 4.1, the healthy skin temperature of the cases S24 and S48 were calculated to be 32.9(±0.1)°C and 33.2(±0.1)°C, respectively. Therefore, both columns of figures in Figure 4.5 show the contour areas with temperature elevation of 2.60°C, 2.75°C, 2.90°C, 3.05°C and 3.20°C(±0.1°C), and the areas can thus be directly compared to see the thermal signature changes of the hemangioma between the two imaging sessions. The marker sizes of the two imaging sessions were 4cm by 4cm and 2cm by 2cm, respectively.

As shown in Figure 4.6 below, areas with the same temperature elevations from the healthy skin temperature from both S24 and S48 were compared. The areas computed for the second imaging session (S48) regressed by an average of 74% compared to those in the first imaging session (S24).

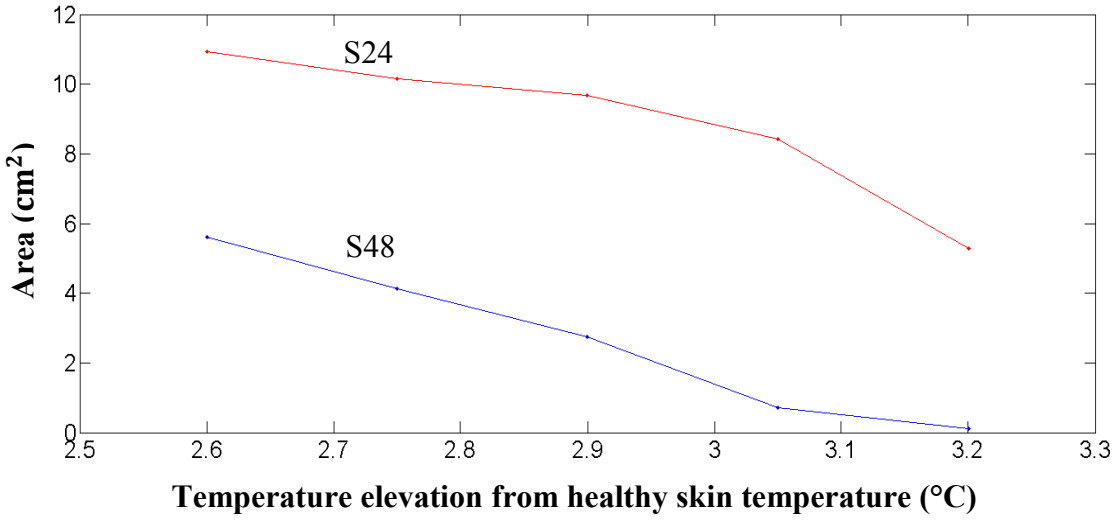

Figure 4.6: Change of areas of corresponding temperature-elevated contours between the imaging sessions of S24 and S48.

The same area analysis was repeated for the two imaging sessions of the second patient (S20 and S39). As is mentioned in Section 4.1, the healthy skin temperature of the cases S20 and S39 were calculated to be 34.2(±0.1)°C and 33.9(±0.1)°C, respectively. Contour areas with temperature elevation of 1.30°C, 1.45°C, 1.60°C, 1.75°C and 1.90°C were compared to see the thermal signature changes of the hemangioma between the two imaging sessions (Figure 4.7). The marker sizes of the two imaging sessions were 3cm by 3cm and 1cm by 1cm, respectively.

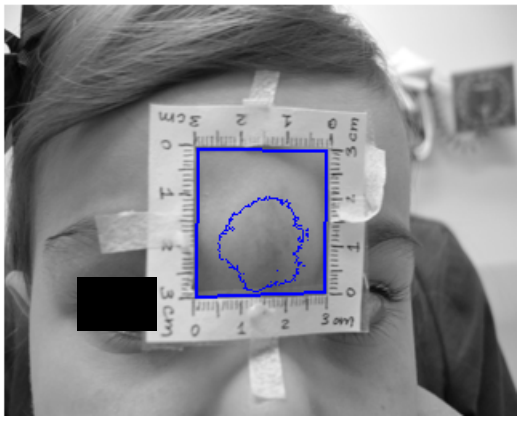

(a)

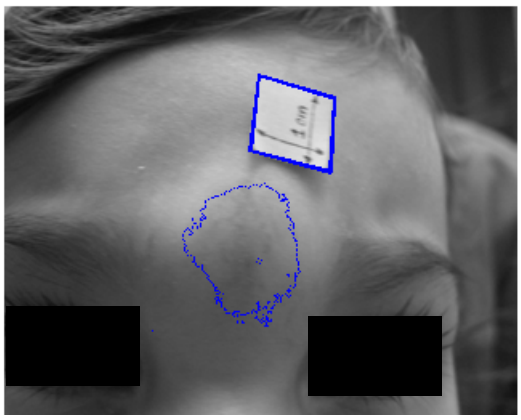

(b)

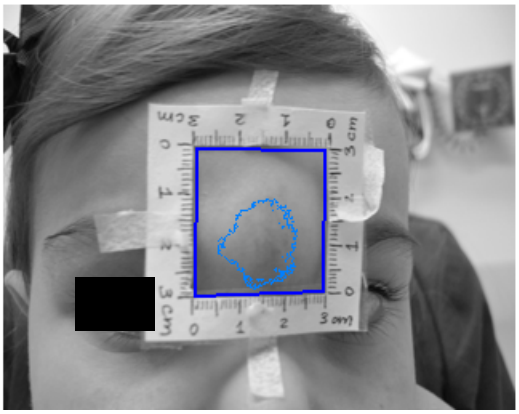

(c)

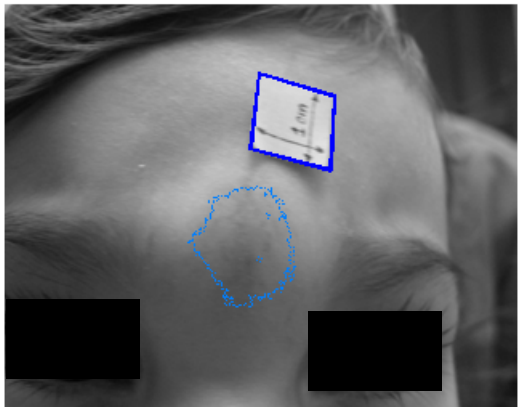

(d)

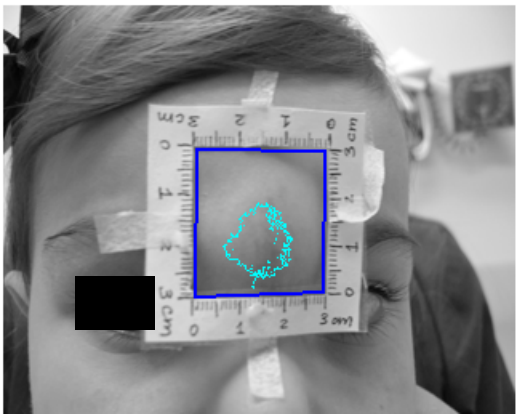

(e)

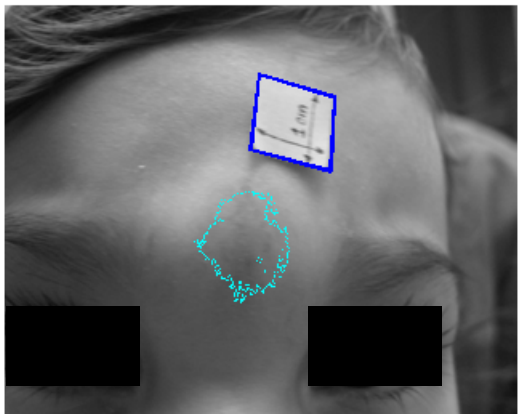

(f)

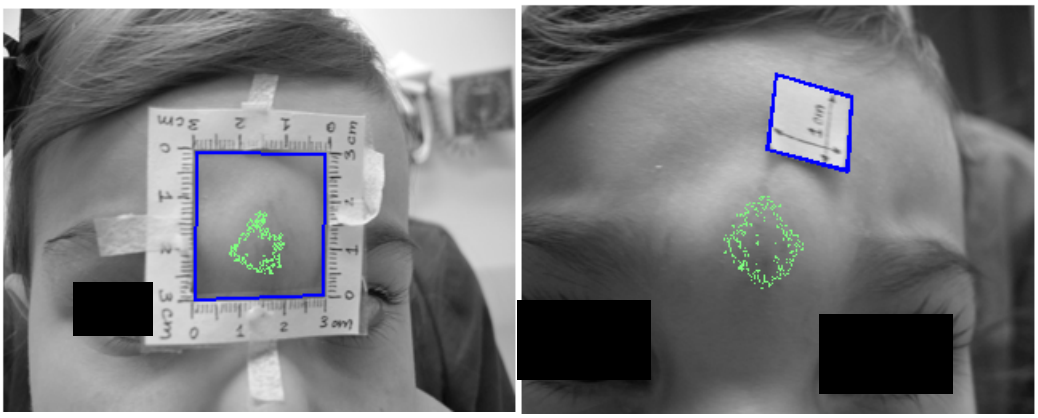

(g) (h)

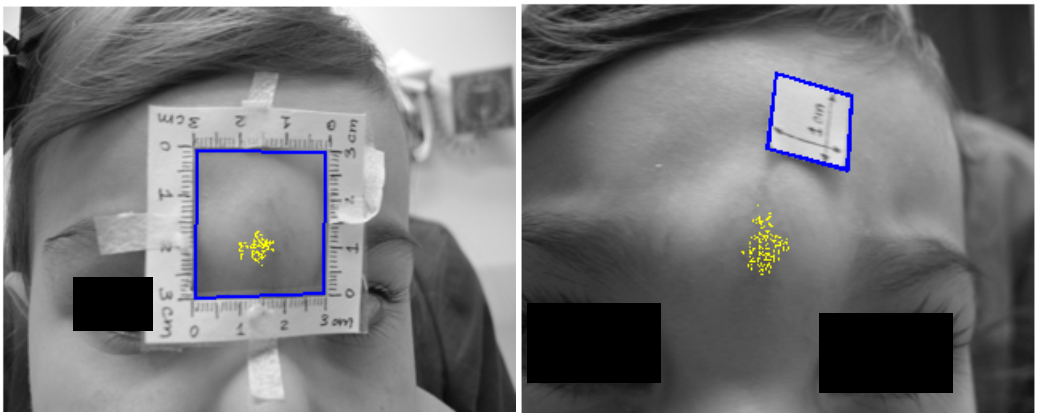

(i) (j)

Figure 4.7: Areas comparison for the same patient during imaging sessions S20 and S39. Areas in pixels were calculated for each of the contours above. Contour lines in Figures (a)(c)(e)(g)(i) represent contour areas of Patient S20 with temperature above 35.50°C, 35.65°C, 35.80°C, 35.95°C, 36.10°C, respectively. The area in pixels of the square box shown in blue was calculated as the marker area in pixels. Figures (b)(d)(f)(h)(j) represent contour areas of Patient S39 with temperature above 35.20°C, 35.35°C, 35.50°C, 35.65°C, 35.80°C, respectively. Each pair of figures in a row is showing contours at the same level of relative temperature elevation (compared to healthy skin temperature) for the two imaging sessions.

As shown in Figure 4.8 below, the correspondent areas in the latter imaging session (S39) regressed by an average of 22% compared to the earlier one (S20).

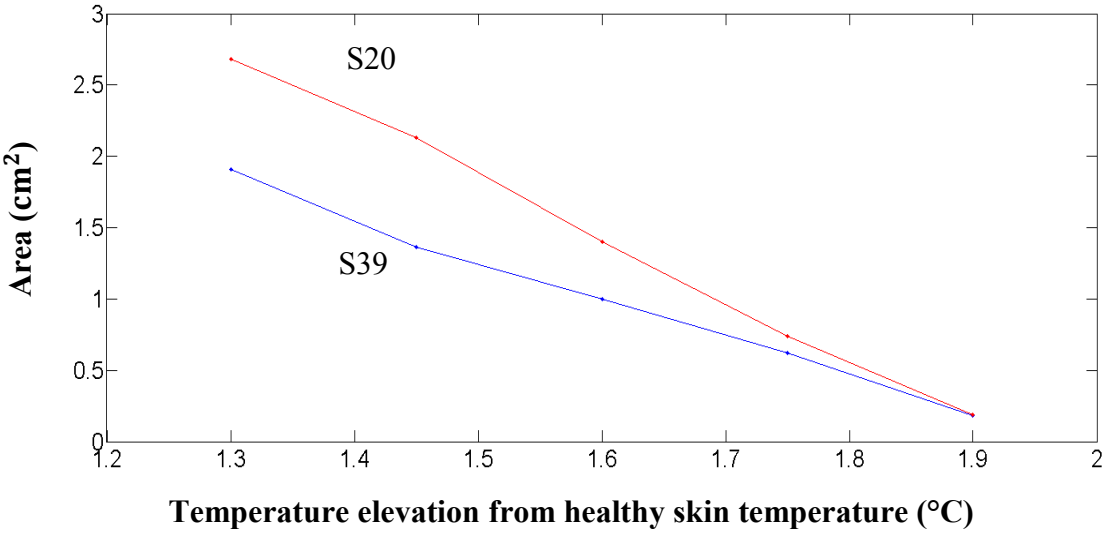

Figure 4.8: Change of areas of corresponding temperature-elevated contours between the imaging sessions of S20 and S39.

5 Notes for future work

5.1 Notes on experiment

The paper marker should be placed in the same plane as the lesion site, which should also be normal to the camera view. Therefore, the paper marker should not be too large in order to avoid a significant curvature when placed on the human body. For example, for the case S24 (Figure 5.1(a)), the paper marker was so large that it was curved to wrap around the arm. The curvature

induced errors to the area calculation because the marker area in pixels could not be determined with high level of confidence.

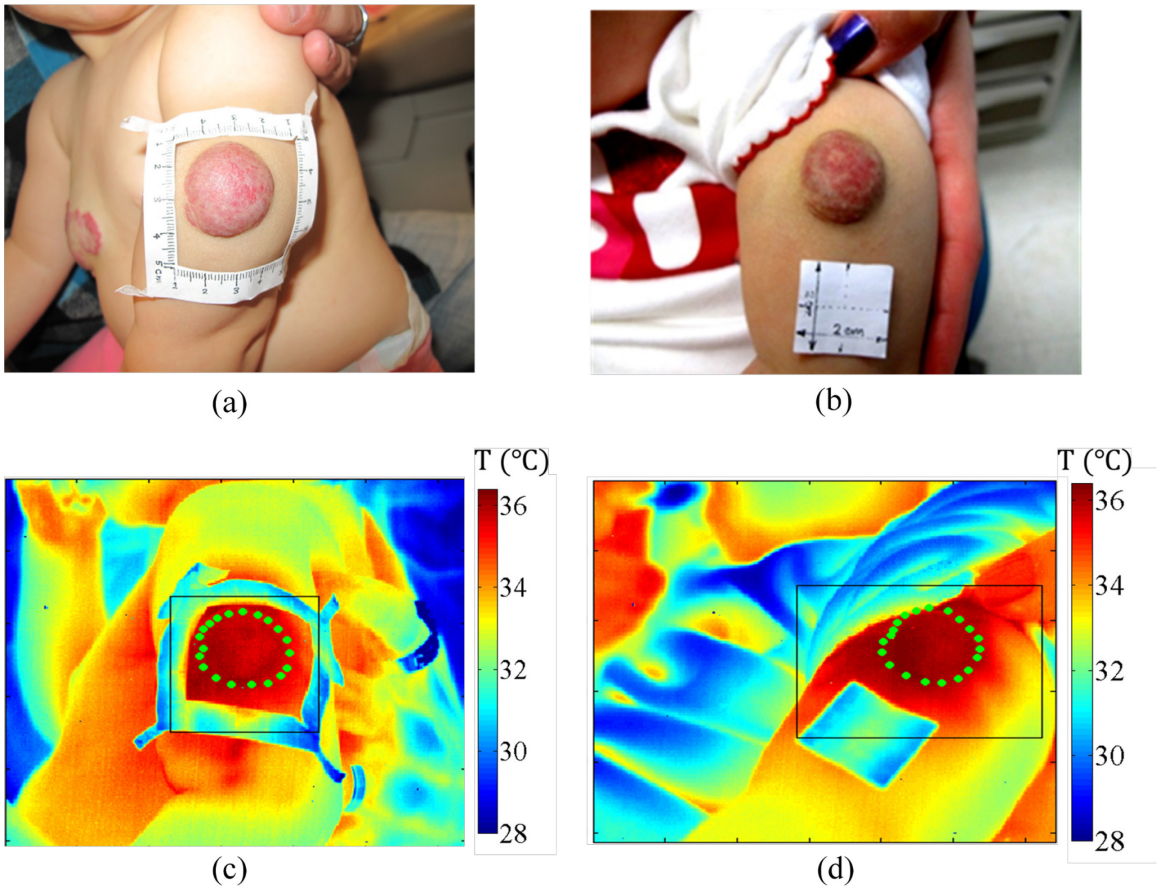

Figure 5.1: Markers in the analysis for S24 and S48. (a) The white-light image of S24. (b) The white-light image of S48, (c) The infrared image of S24, (d) infrared image of S48.

Also, it can be observed from Figure 5.1(c) and (d) that the markers were blocking part of the subcutaneous thermally active regions in both cases. If possible, the paper marker should be placed away from thermally active regions. It is recommended, therefore, to view the thermal signatures through the infrared image beforehand to decide on the marker location.

5.2 Notes on analysis

The temperature measurements were accurate only within certain range of viewing angle (angle between camera axis and surface normal) of the infrared camera. Experimental results have shown that the curvature effect on the accuracy of temperature measurement becomes significant when the viewing angle exceeds 60°. In such cases, corrections based on the directional emissivity should be applied to reduce measurement errors [16].

The segmentation of superficial boundary of the lesion is semi-automatic, which involves manual adjustment of certain parameter during segmentation. The advantage of this method over manually representing the boundary using discrete points is that it gives a complete boundary, while discrete points may induce ambiguity of the boundary. However, the optimal adjustment settings would depend on factors such as lesion shape and photo quality, which are case-dependent. Under some circumstances it may take too much effort in creating a good segmentation semi-automatically (case-dependent), and manually defining the boundary may save time of processing. Also, by manually defining the boundary, it is possible avoid obvious mistakes of the semi-auto segmentation due to low photo quality or contrast. Therefore, given that neither of the methods seem perfect, it is ideal to develop a fully automatic detection algorithm in the future.

The area calculation method used the solution for the TSP optimization as an approximation. Generally, it automatically outlines the polygon representing the area of the given contour line. One major problem is that when the contour area of a certain temperature range is composed of multiple sub-areas, the current algorithm will only be able to approximate them to be one area. For example, as is shown in Figure 5.2, it is possible that such contour should be considered as two sub-areas. In this case, the area in between two areas should not be calculated. Only the sum of the two sub-areas should count toward the contour area. Possible improvements can be made by pre-defining how many clusters are needed, or implement algorithms that find multiple cluster

centers automatically. Another method is to investigate on the original contour given in MATLAB. It may be possible to calculate the area of the superimposed temperature contours based on the original contour in the infrared image.

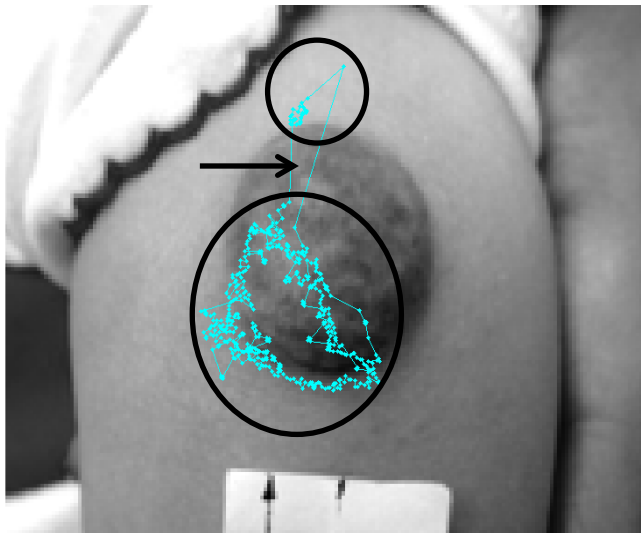

Figure 5.2: Area of a temperature elevation level composed of multiple sub-areas. Possibly two sub-areas were observed, which were marked by the circles. The arrow points to the area between the circles that should not be included in the calculation of the contour area.

The validity of the method used in comparing the areas of the same level of temperature elevation of the same patient between two imaging sessions, relies on the assumption that the healthy skin temperature is well-approximated by averaging temperatures within the chosen areas mentioned in Section 3.2.3, and that healthy skin temperature is universal on the entire region of interest. The comparison of areas with correspondent temperature elevation presents a general idea on the tracking the change of the lesion's thermal signatures.

From the skin temperature detected in the infrared image, a reverse calculation is possible to find local metabolic heat generation caused by the lesion, which may make the analysis results

more direct and more accurate. Such calculation can be achieved by forming a skin tissue heat transfer model similar to the model introduced by Cetingul and Herman [17].

6 Conclusion

Using the infrared thermography, thermal signatures of the infantile hemangioma lesions were assessed quantitatively. The temperature distributions of the lesion and surrounding healthy skin regions were accurately measured. The temperature contours were superimposed onto the white-light image. With this method, subcutaneous lesion elements and the affected areas can be viewed in supplement to the superficial lesion on a single image. It is an effective method to monitor the regression of hemangiomas. The method is also supported by quantitative analyses where areas associated with elevated temperature contours were calculated for successive imaging sessions to deliver data for longitudinal studies. It provided quantification for the regression of hemangioma in addition to the visualization described before. In the two cases analyzed, the corresponding areas of the latter imaging sessions regressed by an average of 74% and 22%, respectively, compared to those of the earlier imaging sessions.

Bibliography

[1] Saxena AK, Schleef J, Morcate JJ, Willital GH (1999) Thermographic imaging of an angioma serpiginosum. Int J Surg Sci 6:156–157

[2] Saxena AK, Willital GH (2001) Hemangioma treatment using lasers and thermographic controls. Acta Chir Austriaca 33:16

[3] Katona G, Csakanyi Z, Gacs E, Szalai Z, Rath G, Gerlinger I (2012) Propranolol for infantile haemangioma: Striking effect in the first weeks. International Journal of Pediatric Otorhinolaryngology, Volume 76, Issue 12 , Pages 1746-1750.

[4] Pennes HH (1948) Analysis of tissue and arterial blood temperature in the resting human forearm J. Appl. Physiol. 1 93–122

[5] Saxena AK, Willital GH (2007) Infrared thermography: Experience from a decade of pediatric imaging. Eur J Pediatr (2008) 167:757–764

[6] Verity DH, Restori M, Rose GE (2006) Natural history of periocular capillary haemangiomas: changes in internal blood velocity and lesion volume. Eye (2006) 20, 1228–1237. doi:10.1038/sj.eye.6702387

[7] Naikmasur VG, Sattur AP, Burde K, Nandimath KR, Thakur AR (2010) Central hemangioma of the mandible: Role of imaging in evaluation. Oral Radiol (2010) 26:46–51. DOI 10.1007/s11282-010-0035-8

[8] Perkinsa JA, Sidhub M, Manninga SC, Ghionib V, Sze R (2005) Three dimensional CT angiography imaging of vascular tumors of the head and neck. Intl J Pediatr Otorhinolaryngol. 2005;69:319–25.

[9] Kalicki B, Jung A, Ring F, Rustecka A, Maslany A, Zuber J, Murawski P, Bilska K, Wozniak W (2012) Infrared Thermography Assessment of Infantile Hemangioma Treatment by Propranolol. EAT2012 Book of Proceedings – Appendix 1 of Thermology international 22/3 (2012)

[10] Cetingul MP, Herman C, Alani RM (2009) Skin imaging with infrared thermography and confocal microscopy. pp. 731-739.

[11] Hartley and Zisserman, Multiple view geometry in computer vision, 2 ed., Cambridge University Press [2004].

[12] The MathWorks Inc., Detecting a cell using image segmentation. http://www.mathworks.com/help/images/examples/detecting-a-cell-using-image-segmentation.html. Accessed on Apr.16, 2014.

[13] Nilsson C. Heuristics for the traveling salesman problem.

[14] Wikipedia. Graham scan. http://en.wikipedia.org/wiki/Graham_scan. Accessed on Apr. 16, 2014.

[15] Description by Cohen B, Grossberg A of the Johns Hopkins Hospital.

[16] Cheng TY, Deng D, Herman C (2012) Curvature Effect Quantificaiton for In-Vivo IR Thermography. IMECE2012-88105, pp. 127-133.

[17] Cetingul MP, Herman,C (2010) A heat transfer model of skin tissue for the detection of lesions: sensitivity analysis. Phys. Med. Biol. 55 (2010) 5933–5951

[18] de Berg M, van Kreveld M, Overmars M, Schwarzkopf O. (2000) Computational Geometry: Algorithms and Applications. Springer, pp. 2–8.

Appendix I

1 Polynomial fit for camera calibration

The relationship between infrared camera image intensity(g) and the blackbody temperature(T) was given for a temperature range of 5°C - 35°C:

$$T(℃) = -53.771 + 0.0045575g - 1.1612 \times 10^{-7}g^2 + 1.692 \times 10^{-12}g^3 - 9.9176 \times 10^{-4}g^4$$

2 Procedure of transforming thermal contours from infrared to white-light image

The white-light and infrared images of patient S48's hemangioma were shown in Figure 2(a) and (b), respectively. The contour map for the ROI as shown in Figure 3(a) has a temperature range of between the healthy skin temperature (in this case, 33.2°C) and the highest temperature within the ROI (36.4°C). To transform these contours onto white-light image, it is key to define the number of colors to be used and what each color represents (colormap). Once desired temperature difference between neighboring contours is decided (in this case, 0.2°C), the colormap is determined given the temperature range. The actual transformation procedure begins with picking out the pixels in the contour that represents the skin with a temperature between 33.2°C and 33.4°C. The two-dimensional projection was performed for these pixel coordinates using Equation 4. The pixels were filtered so that only those within the ROI were left. Next, these pixels were plotted onto their corresponding locations in the white-light image, and were shown using the pre-determined color. The actual temperature range plotted was from 33.2°C to 33.39°C in order to avoid repeated plotting between neighboring contours. The same procedure was repeated until the projection for all 16 contours, from 33.2 °C to 36.4 °C, was completed (Figure

I(a)-(e)). A duplicate of Figure I(a) was finally overlaid with certain transparency in order to simultaneously view the superficial lesion and the thermal contours around it(Figure I(f)). The superficial boundary was outlined for further clarity.

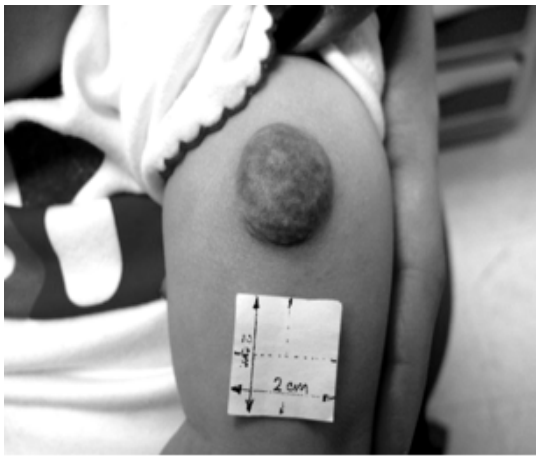

(a)

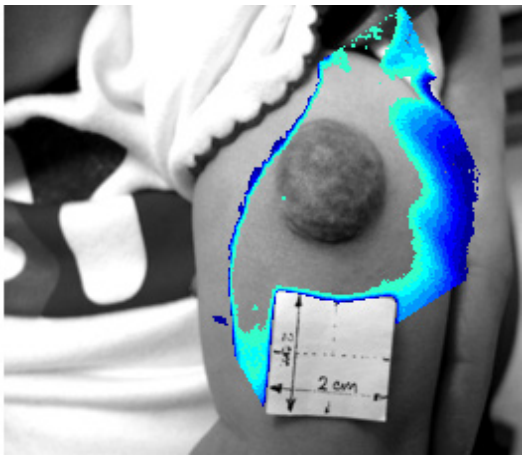

(b)

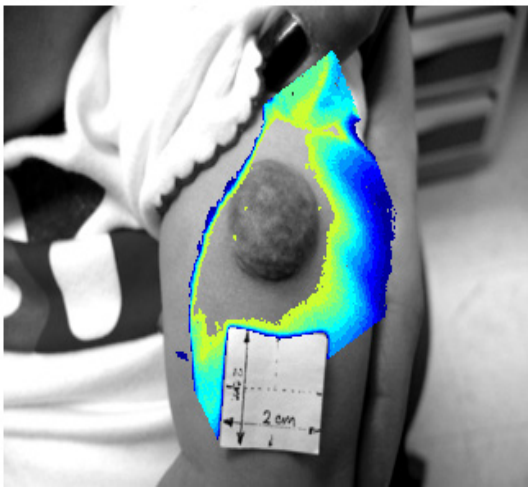

(c)

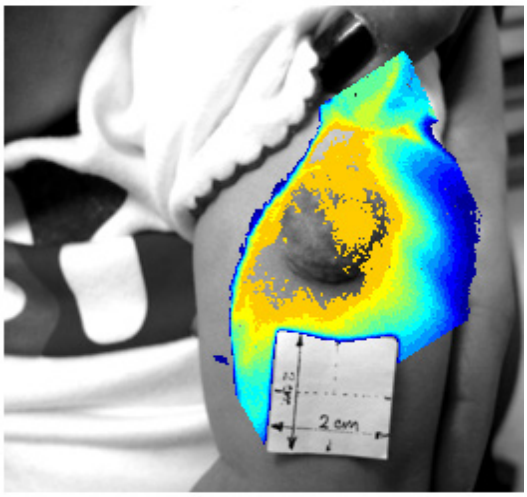

(d)

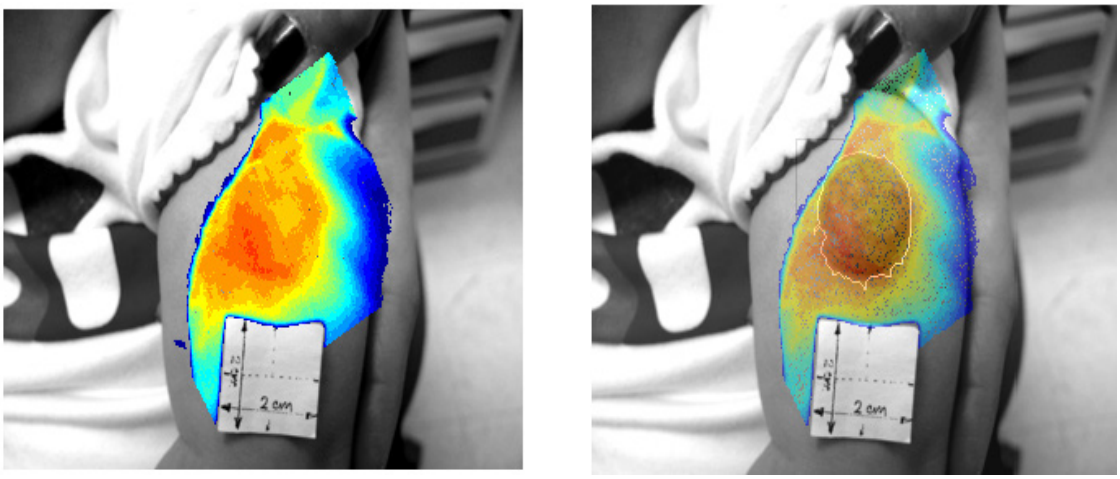

(e) (f)

Figure I.1: Procedure of transforming thermal contours from infrared to white-light image.

(a) White-light image of the hemangioma. (b)-(e) The projection of the thermal contours onto to the white-light image, beginning with a contour representing 33.2-33.4°C, and proceeding with contours, each representing a range of 0.2°C, until the final contour representing 36.2-36.4°C was reached (All sixteen contours are shown in image (e), and these figures were chosen to represent the whole process). (g) The white-light image was made transparent and laid on top of the temperature contours; the boundary of the hemangioma's superficial component was outlined in white.

3 Procedure of segmentation of superficial lesion boundary

The gradient image can be calculated, and a threshold can be applied to show the desired range of "edges", which forms Figure I.2(b). This threshold was manually determined for each case. Then all elements in the image were dilated in different directions depending on how good

it distinguish the lesion from the background (Figure II(c)). After that, holes in the interior of the lesion was filled (Figure II(d)), and outlying elements were removed (Figure II(e)).

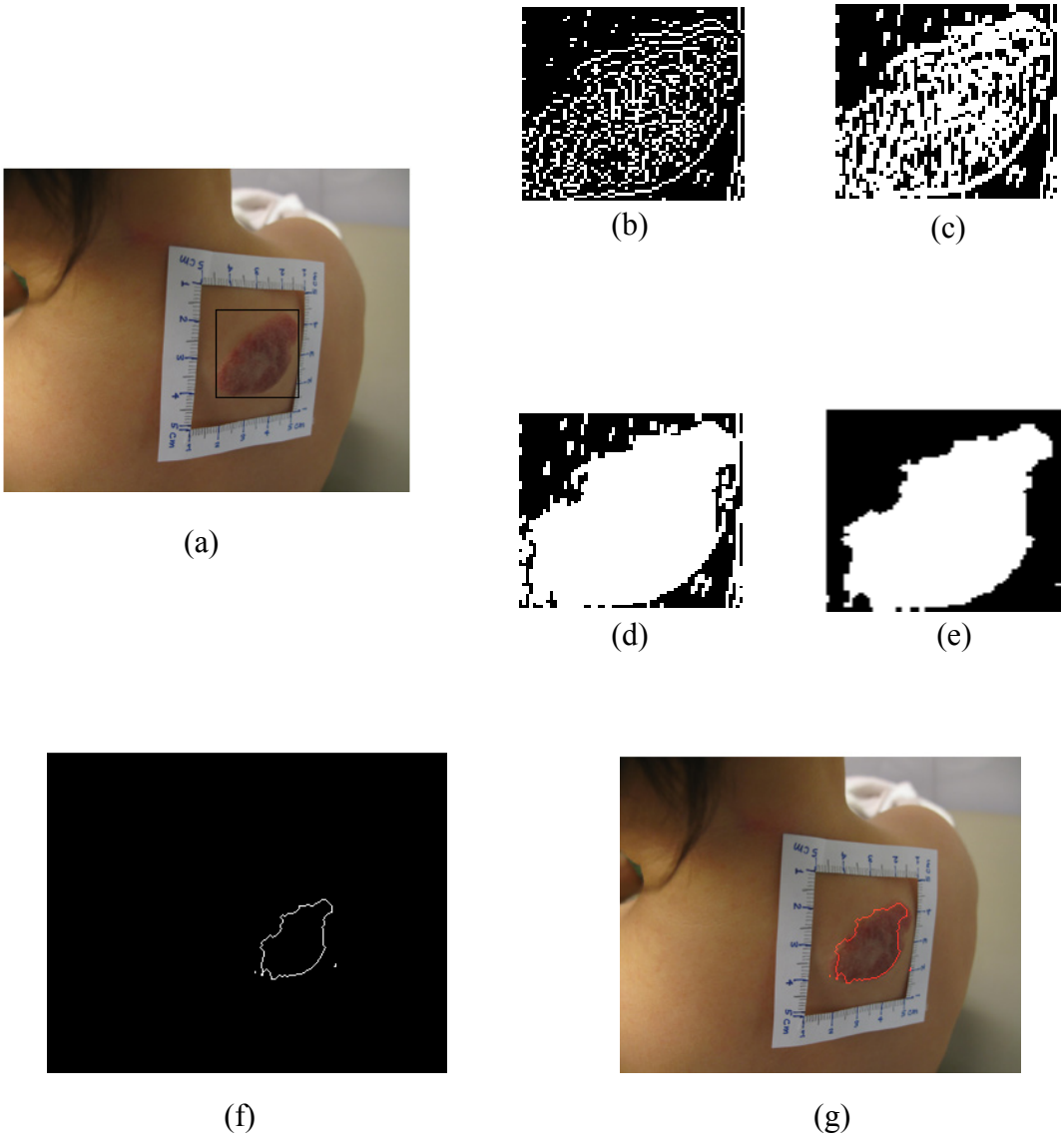

Figure I.2: Semi-auto segmentation of lesion superficial boundary. (a) (f) (g) are identical to Figure 3.5(b). Greyscale gradient with a threshold applied. (c) Dilation on vertical direction. (d) Binary closing, filling small elements inside lesion. (e) Binary opening, emptying small elements outside lesion.

Appendix II

1 Convex hull and the Graham scan

Mathematically, the convex hull of a set of points *S* is the smallest convex set containing *S*. We may imagine stretching a rubber band so that it surrounds the entire set *S* and then releasing it, allowing it to contract; when it becomes taut, it encloses the convex hull of *S* [18].

The Graham scan is a method of computing the convex hull of a finite set of points in the plane with time complexity O($n \log n$). The algorithm finds all vertices of the convex hull ordered along its boundary [14]. The following version of the Graham scan algorithm is implemented in this study. For example, given a point set *S* below in Figure II.1, it first searches for the point in the set that has the smallest y-coordinate (Point P). Then it connects all other points in the set to P, and finds the angles between all these lines and the positive x-direction. Next, it sorts all the points in the ascending order of the angle to get a sorted set *S'*. The scan starts adding three points, which are P and the first two points in *S'*, to the convex hull. At each iteration step, it finds out whether the latest three points added to the convex hull form a "left turn" or a "right turn". If it is a "left turn", the algorithm continues to add the next point in *S'* to the convex hull. If it is a "right turn", then the second to last point in *S'* will be removed from the convex hull. This iteration continues as long as the three latest points in the convex hull form a "left turn". After all the points in *S'* are scanned, the result is the convex hull of the point set S.

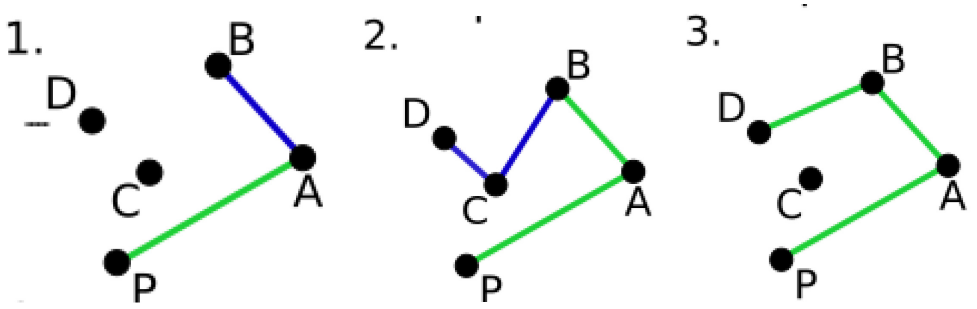

(a) (b) (c)

Figure II.1: Graham scan algorithm to find convex hull of a set of points. (a) The scan starts from points P, A and B. (b) The scan attempts to add points C and D to the convex hull. (c) C is left out from the convex hull because a "right turn" occurred on the path B-C-D.

Vita

Xinrong You was born in Shanghai, China on February 3rd, 1990. He received his Bachelor of Science degree in Mechanical Engineering from University of Michigan, Ann Arbor, in 2012. He also received his Bachelor of Science degree in Electrical and Computer Engineering from Shanghai Jiao Tong University in 2012.